Soft Matter

Accepted Manuscript

This is an Accepted Manuscript, which has been through the Royal Society of Chemistry peer review process and has been accepted for publication.

Accepted Manuscripts are published online shortly after acceptance, before technical editing, formatting and proof reading. Using this free service, authors can make their results available to the community, in citable form, before we publish the edited article. We will replace this Accepted Manuscript with the edited and formatted Advance Article as soon as it is available.

You can find more information about Accepted Manuscripts in the author guidelines.

Please note that technical editing may introduce minor changes to the text and/or graphics, which may alter content. The journal's standard Terms & Conditions and the ethical guidelines, outlined in our author and reviewer resource centre, still apply. In no event shall the Royal Society of Chemistry be held responsible for any errors or omissions in this Accepted Manuscript or any consequences arising from the use of any information it contains.

ROYAL SOCIETY OF CHEMISTRY

rsc.li/soft-matter-journal

Journal Name

ARTICLE

Impact of Solution Phase Behaviour and External Fields on Thin Film Morphology: PCBM and RRa-P3HT model system

ceived 00th January 20xx,
Accepted 00th January 20xx

DOI: 10.1039/x0xx00000x

www.rsc.org/

A. A. Y. Guilbert[a] and J. T. Cabral[a]

We report the impact of the ternary solution phase behaviour on the film morphology and crystallization of a model polymer:fullerene system. We employ UV-Vis absorption spectroscopy, combined with sequential filtration and dilution, to establish the phase diagram for regio-random poly(3-hexylthiophene-2,5-diyl) and phenyl-C61-butyric acid methyl ester (PCBM) in chlorobenzene. Films are systematically cast from one- and two-phase regions decoupling homogeneous and heterogeneous nucleation, and the role of pre-formed aggregates from solutions. Increasing annealing temperature from 120 to 200°C reveals a highly non-monotonic nucleation profile with a maximum at 170°C, while the crystal growth rate increases monotonically. UV ozonolysis is employed to vary substrate energy, and found to increase nucleation rate and to promote a binary crystallization process. As previously found, exposure to light, under inert atmosphere, effectively suppresses homogeneous nucleation; however, it has a considerably smaller effect on heterogeneous nucleation, either from solution aggregates or substrate-driven. Our results establish a quantitative link between solution thermodynamics, crystallization and provide insight into morphological design based on processing parameters in a proxy organic photovoltaic system.

[a] *Centre for Plastic Electronics and Department of Chemical Engineering, Imperial College London, London SW7 2AZ, United Kingdom.*

Electronic Supplementary Information (ESI) available: optical micrographs, atomic force micrograph, kinetics analysis of nucleation and growth, UV lamp spectrum and contact angle measurements. See DOI: 10.1039/x0xx00000x

1. Introduction

Manufacturing polymer nano-composite films, at low cost and large scale, is key to numerous industrial applications ranging from membranes and coatings to organic electronics. While the spontaneous assembly of polymer and small molecules from solution provides an attractive route to low manufacturing costs by reducing the number of processing steps (ideally to a single deposition step),[1] it requires an understanding of multicomponent thermodynamics and (non-equilibrium) pathways to film formation. Conjugated polymer/fullerene/solvent mixtures are particularly significant for organic photovoltaic (OPV) applications since OPV device performance is strongly determined by the microstructure of the active layer.[2]

The impact of processing variables such as solubility,[3-4] solvent or mixture of solvents,[5] thermal and solvent annealing,[6] miscibility,[7] polymer regioregularity and molecular weight[8] has been extensively studied. However, the phase behaviour of the polymer/fullerene/solvent ternary mixtures remains largely elusive, since research efforts have been primarily focused on the resulting film morphology. In this paper, we examine the impact of solution phase behaviour on fullerene crystallisation and thin film morphology (Figure 1).

Previous studies on the model ternary system polystyrene/C_{60} fullerene/toluene revealed that the polymer conformation remained unchanged upon addition of C_{60} while addition of polymer induced fullerene aggregation.[9] The resulting microstructure was shown to depend on the state of the solution and on the deposition technique (spin-coating vs drop-casting). Interestingly, the same behaviour was observed with phenyl-C61-butyric acid methyl ester (PCBM) in relatively poor solvent (toluene) but not in good solvent (chlorobenzene).[10§]

We selected as model system (Figure 1) an amorphous conjugated polymer regiorandom poly(3-hexyl)thiophene (RRa-P3HT), a soluble fullerene derivative, PCBM and a good solvent for PCBM, chlorobenzene (CB). RRa-P3HT was employed, instead of the ubiquitous regioregular P3HT, which is directly relevant for OPV applications, in order to probe the direct impact of the phase behaviour in solution on PCBM crystallisation without having to disentangle it from the impact of the polymer crystallisation, which is known to happen more readily from solution.[11] We reported previously the binary RRa-P3HT:PCBM phase diagram.[12]

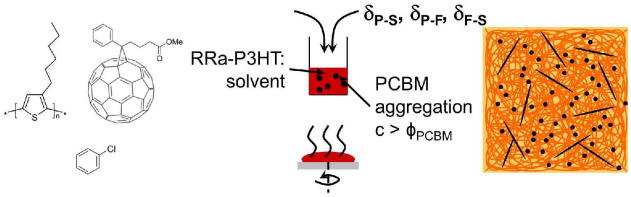

Figure 1. Scheme representing the impact of RRa-P3HT/PCBM/CB phase behaviour and drying pathways (e.g. via spin coating) on the resulting polymer:fullerene blend microstructure.

2. Results

Ternary phase diagram

In solution processable OPVs, the solubilities of the various components in the pure solvent and in the ternary mixture are thought to be critical parameters for processing. From a thermodynamic viewpoint, solubility of a component is defined as the concentration of solute for which the rate of dissolution equals the rate of precipitation. Evidently, the rates of dissolution and precipitation near the solubility limit become very slow, contributing to the difficulty in precisely measuring phase boundaries. We tackled this issue using our model system, with a combination of spectroscopy, filtration and dilution.

Both polymer and fullerene are strong absorbers (in the visible for the polymer and in the UV for the fullerene) and thus UV-Vis absorption spectrometry can be used to measure accurately their concentration in dilute solution, within a given composition range. Absorbance and concentration in solution were readily related by measuring calibration curves, shown in Figure 2, and using the Beer-Lambert law, $A = \varepsilon\, l\, c$, where A is the absorbance, ε is the molar absorptivity, l is the light path distance and c the concentration of the solution, corresponding to a light transmittance of $T=10^{-A}$. This led to a molar absorptivity of $7.5.10^2$ m^2/mol for RRa-P3HT at 434 nm and of $1.4.10^2$ m^2/mol for PCBM at 500 nm.

To measure the solubility, we borrowed a method used extensively in the pharmaceutical industry: the saturation shake-flask method.[13] Solutions containing a solute excess were stirred overnight at the chosen temperature before separating the saturated solution and the precipitate by filtration (PTFE membrane filter with pore size of 0.2 μm). Filtration was chosen over centrifugation here since, in practice, it is common to filter solution prior to thin film deposition to remove any undissolved materials or impurities. The concentration of the filtered solution thus corresponded to the solubility limit; however, its absorbance was frequently above the concentration range where it could be rigorously measured spectroscopically. The filtered solutions were therefore diluted to measurable concentrations in the range depicted in Figure 2, and as illustrated in Figure 3. In order to increase measurement accuracy, different PCBM concentrations [PCBM] in solution were investigated (20 to 60 mg/ml) and the light path reduced by using a 1mm thick quartz cuvette, which enabled the measurement of relatively high concentrations of RRa-P3HT (up to 0.5 mg/ml). UV-Vis spectrometry enabled the simultaneous measurement of the concentration of both components in the filtered solution since at such low concentrations, the absorbance spectra of the blend could be fitted by a linear combination of the molar absorptivity of the neat components (see Figure 3 a), extracted from the calibration curves (see Figure 2 c and f). The master curves used to determine the solubility of PCBM in solution are plotted in Figure 3 c.

Within the range of polymer:fullerene ratio explored here (down to 3:2), the PCBM solubility limit was always reached for concentrations much lower than RRa-P3HT (we observed the gelation of RRa-P3HT in chlorobenzene for concentrations higher than 130 mg/ml). The resulting ternary phase diagram is plotted for two temperatures, 20°C and 75°C, in Figure 3. As expected, a larger fullerene amount could be dissolved

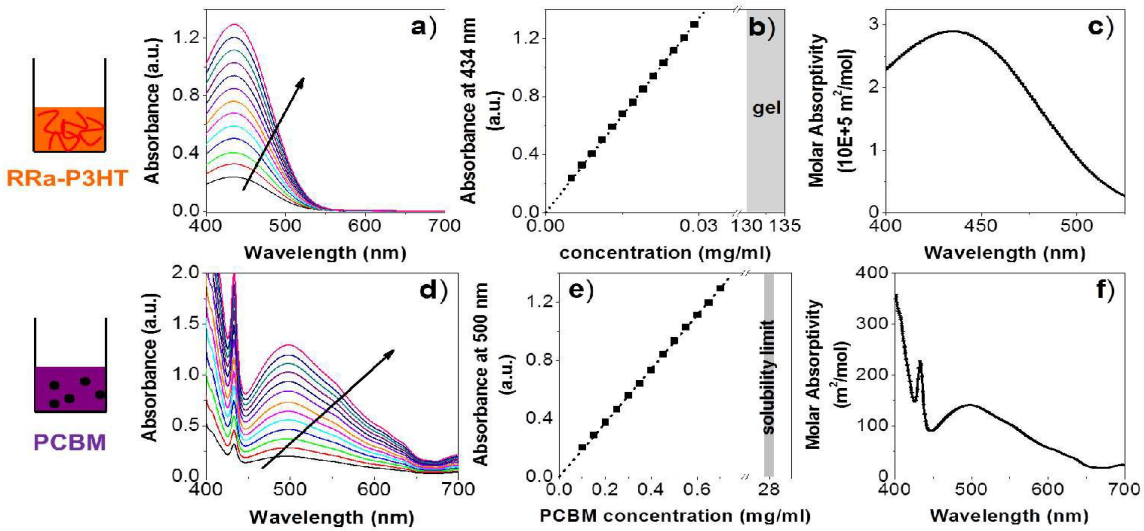

Figure 2. (a,d) Absorbance spectra, (b,e) absorbance-concentration linear relationship and (c,f) molar absorptivity for (a-c) RRa-P3HT and (d-f) PCBM in CB.

when the solution was stirred at 75°C. Further, we measured the 75°C solutions immediately after stirring (for 10 hours) and after allowing the solutions to rest for one week at room temperature, finding the same solubility limits in both cases. This result is surprising and interpreted as due to the asymmetry of dissolution and precipitation rates, and the proximity to the solubility limit at room temperature.

Interestingly, the addition of polymer did not shift the fullerene solubility, within measurement error. Replacing the solvent by polymer, left the PCBM solubility unchanged. This is tentatively explained by the relatively small asymmetry in solvent quality, in line with our previous findings.[10]

Impact of solution phase behaviour on film morphology and PCBM crystallisation.

Effect of PCBM solubility on PCBM crystal nucleation. The area between the blue and the red line in the ternary phase diagram of Figure 3 was particularly interesting because it provided the opportunity to evaluate the impact of solubility on the resulting thin film microstructure at fixed polymer:fullerene ratio and concentration in solution. Depending on the temperature at which the solution was prepared, 30 mg/ml of PCBM in CB belonged to either the one-phase (75°C) or two-phase (20°C) region of the phase diagram. We cast thin films from solutions belonging to both regions, as shown in Figure 4. Since all solutions were cooled to room temperature before casting thin films, these results are directly comparable.

While the as-spun films, cast from the solution prepared at 75°C, were smooth and featureless, the as-spun films cast from solutions prepared at 20°C exhibited large PCBM aggregates, evidently originating from solution. Upon annealing at 160°C under vacuum, films cast from the (one-phase) solutions prepared at 75°C exhibit very few PCBM

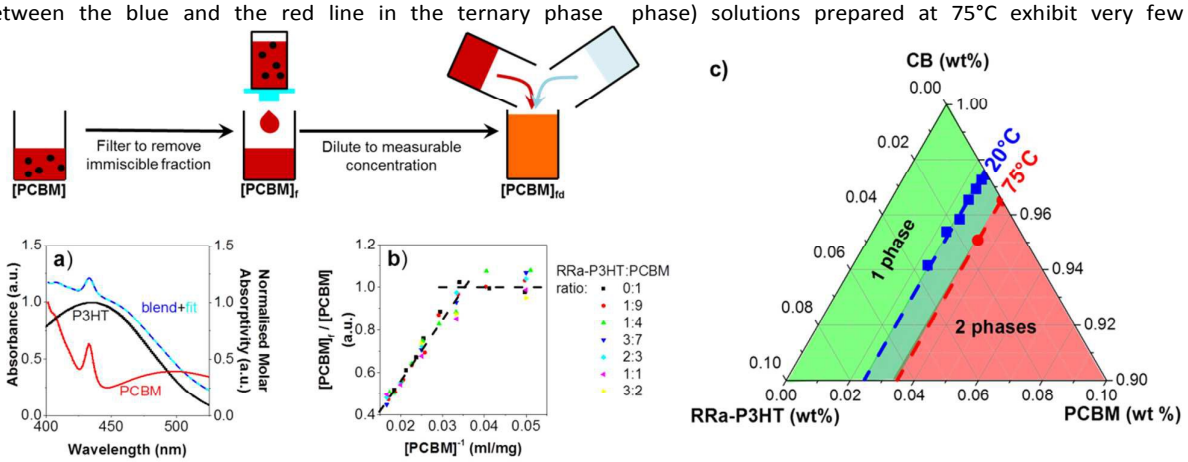

Figure 3. Scheme representing the solubility measurement steps. [PCBM] is the initial PCBM concentration in CB. $[PCBM]_f$ is the PCBM concentration in CB of the filtered solution. $[PCBM]_{fd}$ is the PCBM concentration in CB of the filtered solution after dilution to measurable concentrations by UV-Vis absorption spectrometry. (a) Absorbance spectra of the blend and fit of the absorbance spectra of the blend using a linear combination of the molar absorptivity of the neat components. (b) Normalised PCBM concentration of the filtered solution $[PCBM]_f$ by the initial PCBM concentration [PCBM] as a function of the initial concentration [PCBM] for various polymer:fullerene ratios. (c)RRa-P3HT/PCBM/CB ternary phase diagram at room temperature and at 75°C. The scattered data are from UV-Vis absorption spectrometry. The green region corresponds to concentrations where the system is in one phase while the red region corresponds to concentrations where solution and PCBM solids coexist.

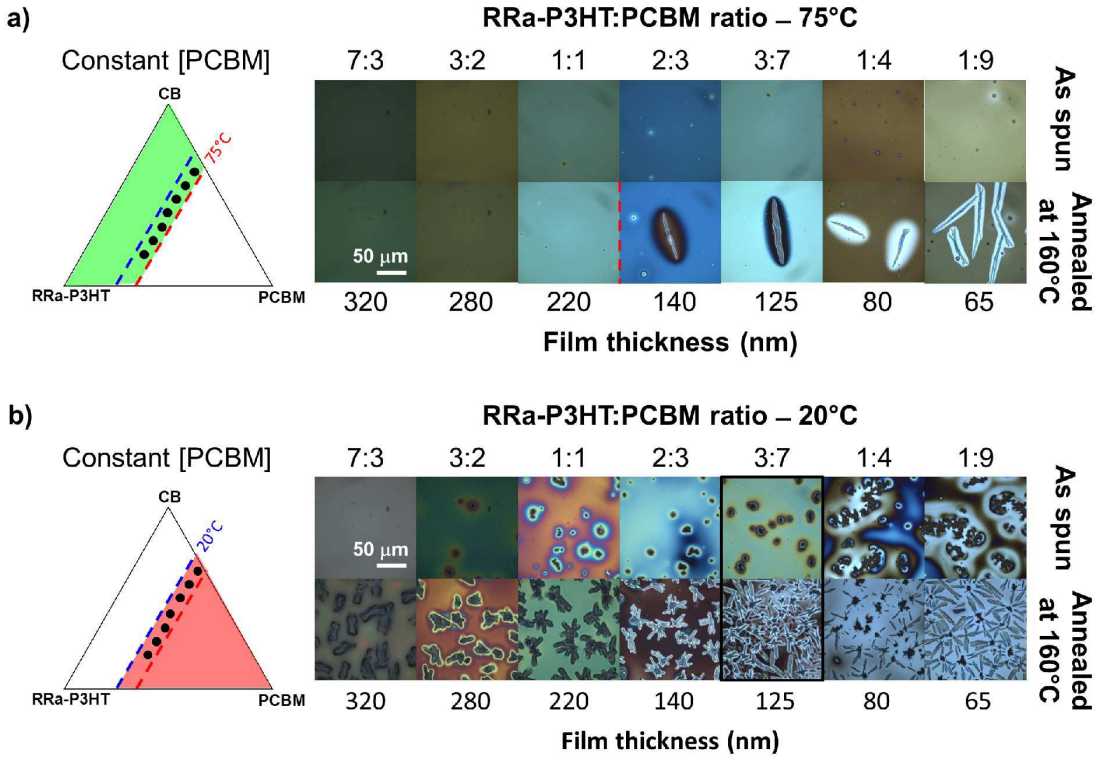

Figure 4. Optical micrographs of RRa-P3HT:PCBM thin films as-spun and annealed at 160°C under vacuum cast from solutions of 30 mg/ml of PCBM in CB prepared at (a) 75°C and (b) 20°C. The polymer:fullerene ratio is varied and thus the film thicknesses vary accordingly. The other processing parameters are kept the same. AFM measurements of the samples prepared at 20°C are provided in Figure S1 in Supplementary Information.

crystals down to 1:4 polymer:fullerene ratio. By contrast, the thin films cast from (two-phase) solutions prepared at room temperature exhibited numerous crystals regardless of the polymer:fullerene ratio. These results indicated that PCBM aggregates present in solution could act as seeds, facilitating the heterogeneous nucleation of PCBM crystals in the thin film. From time-dependent measurement on samples cast from solutions prepared above the solubility limit at 20°C, we clearly observed that crystallisation occurred radially from the aggregates in solution (representative kinetics and morphology examined in Supplementary Information Figure S2 and Figure S3). Homogeneous nucleation, leading to well defined needles as expected for PCBM, was only seen for polymer:fullerene ratio lower than 2:3, but with a much lower frequency in comparison with heterogeneous nucleation. The larger sizes of crystals nucleated homogeneously, from the 75°C solutions, evidenced that growth was favoured over nucleation, at all compositions studied (see Figure 4).

For samples prepared from 20°C solutions, homogeneous and heterogeneous nucleation competed at polymer:fullerene ratios lower than 3:7. Heterogeneous nucleation became less favourable at 1:9 polymer:fullerene ratio. Note that the PCBM aggregates from solution at 1:9 polymer:fullerene ratio displayed larger sizes than those at higher polymer:fullerene ratio and thus, might have been too large to act as efficient nucleating agents. At very low polymer:fullerene ratio (1:9), secondary nucleation took place as seen in Figure 4 (and Supplementary Information Figure S4).

The crystal shape from heterogeneous nucleation events varied from needles at low polymer:fullerene ratio, to “flowers” and then “chromosomes” at high polymer:fullerene ratio. However, film thickness also varied with polymer:fullerene ratio in these experiments, and is known to impact crystal morphology.

Effect of solution concentration on film microstructure. We next investigated thin films of the same polymer:fullerene ratio (3:7), but now systematically varying the fullerene solid content in CB (Figure 5). A clear difference was observed between annealed thin films cast from concentrations in the two- and one-phase regions. Above the solubility limit of PCBM, crystallisation proceeded by heterogeneous nucleation and led to a 3 fold increase in the crystal number density. Further crystal growth became limited by crowding.

Below the solubility limit, nucleation was infrequent and occurred homogeneously (except at low fullerene solid content in CB, as thus thinner films). As shown earlier (Figure 3), aggregation is not likely to happen spontaneously at the short spin-coating deposition time scales. Therefore, the favoured homogeneous nucleation at low fullerene concentration in CB is likely due to film confinement (<15 nm) as diffusion is restricted and thus, nucleation is favoured over

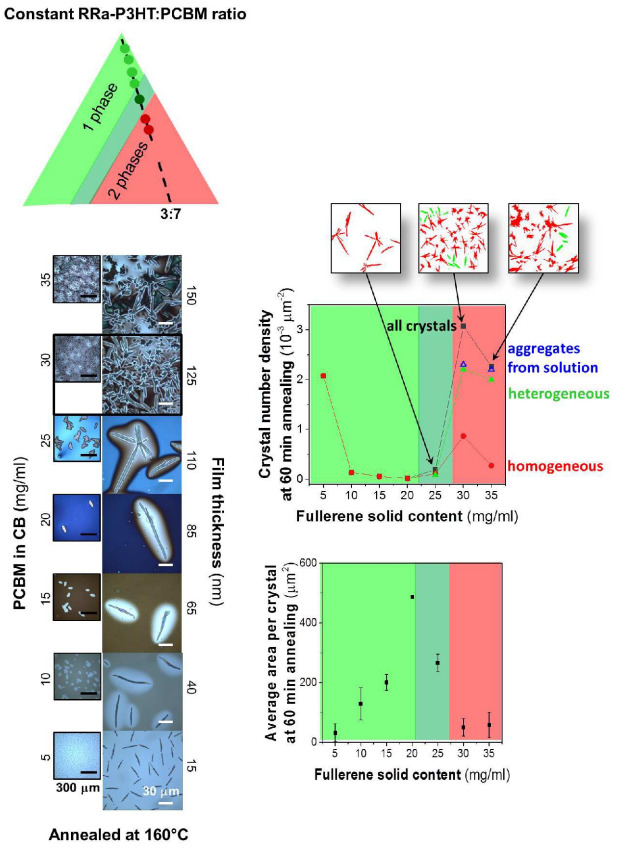

Figure 5. Optical micrographs of 3:7 RRa-P3HT:PCBM thin films annealed at 160°C under vacuum cast from solutions of various PCBM concentration in CB. Crystal number density and single crystal area as a function of fullerene solid content. The insert represents the thresholding; heterogeneously nucleated crystals are coloured in red and homogeneously nucleated crystals are coloured in green.

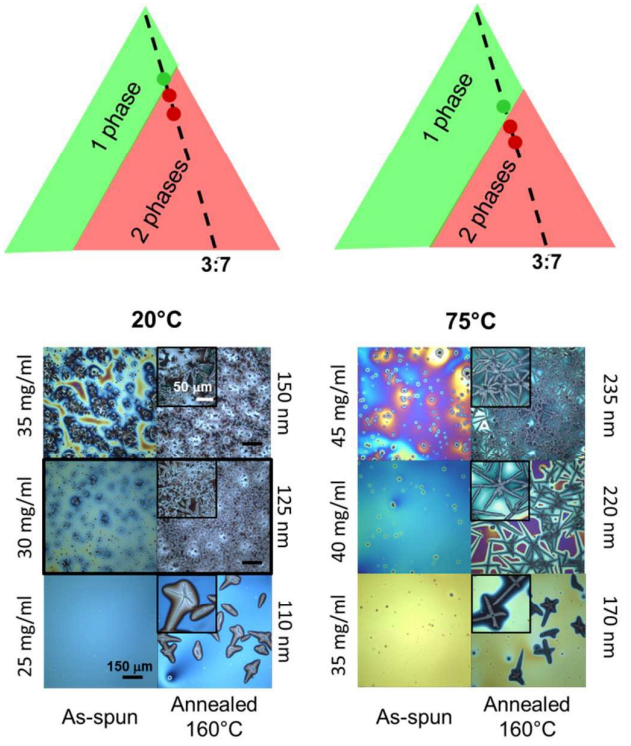

Figure 6. Optical micrographs of as-spun and annealed at 160°C under vacuum of 3:7 RRa-P3HT:PCBM cast from solution of different PCBM concentration in CB above and close to the solubility limit. The solutions have been prepared at room temperature and 75°C.

growth. Close to the solubility limit (20 mg/ml PCBM in CB), crystal shapes were no longer isolated needles, as observed for homogeneous nucleation,[§§] and instead tended to grow radially. Growth rates increased with sample thickness as diffusion was expected to be enhanced.

In order to decouple the effect of solution concentration and film thickness, we carried out a series of experiments varying spin speed profile for the same reference solutions (Supporting Information Figure S5). Acceleration was varied from approximately 100 to 10000 rpm^2. An inverse dependence of nucleation and growth rates with thickness was confirmed, as thicker films yielded larger but fewer crystals.

Effect of PCBM aggregation in solution on film microstructure. Varying the temperature at which the solution was prepared enabled not only to move the phase boundaries of the ternary system but also to tune the number and size distribution of the PCBM aggregates in solution as evidenced from optical micrographs of the as-spun thin film cast above the solubility limit for solutions prepared at 20°C and 75°C (Figure 6). When annealed at 160°C under vacuum, larger and more regular crystals were observed for the films cast from solution prepared at 75°C. The reduction of the number and size of the aggregates led to a dense network of large interconnected crystal structures (Figure 6).

We suggest that heterogeneous nucleation from pre-formed PCBM aggregates in solution represent an attractive route for crystal engineering. Varying the polymer:fullerene ratio enabled to tune the crystal shape. The size of the aggregates in solution did impact the likelihood of the heterogeneous nucleation as seen when the polymer:fullerene ratio was decreased or the temperature of the solution preparation was varied. Decreasing the number of aggregates led to less heterogeneous nucleation centre and thus, enabled better control by tuning the growth of the crystals as evidenced in Figure 6.

Impact of external fields on film microstructure and PCBM crystallization

External fields are known to influence crystal formation in thin films by inducing segregation of components to interfaces, inhibiting homogeneous nucleation, or providing sites for heterogeneous nucleation crystals. Here, we focus on the impact of temperature, substrate treatment and visible light exposure under nitrogen.

Effect of thermal annealing temperature on PCBM crystallization. We first considered the impact of annealing temperature on the nucleation and growth of PCBM crystals.

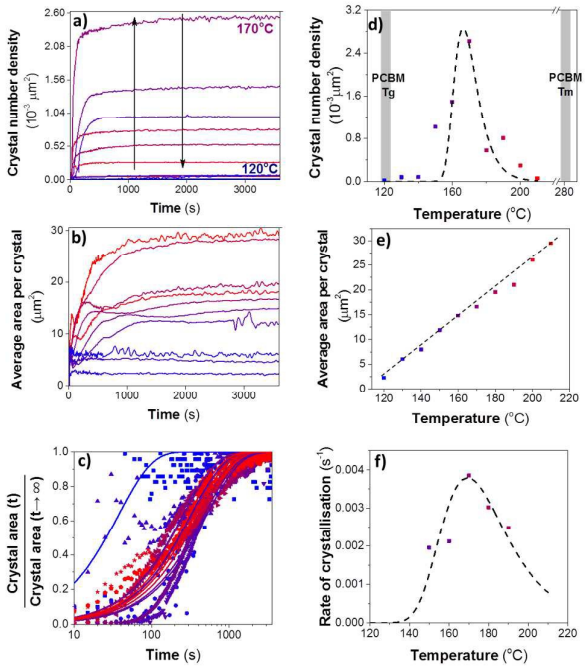

Figure 7. Temperature dependence of crystallization kinetics for 3:7 RRa-P3HT:PCBM sample cast from 10 mg/ml PCBM in CB (prepared at 20°C), within the one phase region. (a) Crystal number density over time, at various temperatures. (b) Average area per crystal over time, at various temperatures. (c) Overall crystallisation kinetics at various temperatures, fitted with an Avrami law $1-\exp\left(-\frac{t^{\beta}}{\tau}\right)$ with β=1. (d) Crystal number density after 60 min annealing time, as a function of temperature; the line is a guide to the eye. (e) Average area per crystal, after 60 min annealing, as a function of temperature. (f) Avrami rate τ, for various temperatures. The optical micrographs at 60 min are provided in Supporting Information (Figure S6). The glass transition temperature Tg and the melting temperature Tm for PCBM are taken from reference.[15]

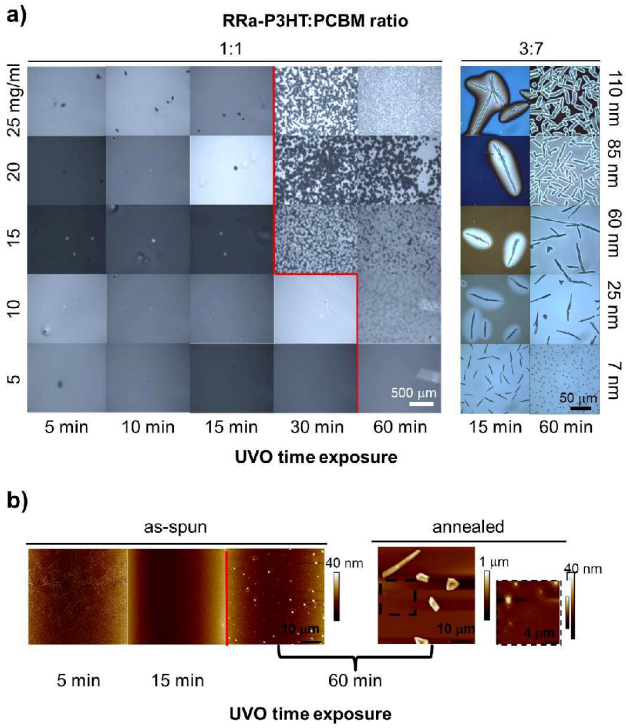

Figure 8. (a) Optical micrographs of 1:1 and 3:7 RRa-P3HT:PCBM cast from solution of different PCBM concentration in CB. The SiOx surface was treated with UVO at varying exposure times. All the samples have been annealed under vacuum at 160°C. (b) Selected AFM scans for 1:1, 20 mg/ml solutions within the one-phase region, depicting the as spun nano-sized aggregates and coexistence with micron-sized crystals upon thermal annealing.

In Figure 7, it can be observed that both nucleation and growth rates are large within this temperature range. The crystal number density exhibits a sharp maximum for a temperature of 170°C. The single crystal area grows monotonically with the temperature, indicative of a smoothly varying growth rate with temperature. This surprisingly sharp peak of the crystal number density has already been observed for other conjugated polymer:fullerene systems.[14]

Effect of substrate treatment on PCBM crystallization. It has been previously reported that substrate energy and roughness can dramatically impact fullerene crystallisation. Here, we used a common UVO treatment to modify the surface properties of SiOx substrates. By varying the time exposure to this treatment, we could vary continuously the substrate free energy.[16] At 1:1 RRa-P3HT:PCBM and a UVO treatment of 15 min, crystallisation was not observed previously for solid content below the solubility limit.[§§§] At a UVO time exposure of 30 min (Figure 8), crystallisation occurred first for PCBM solid content in CB higher than 15 mg/ml and then, for 60 min UVO, at all PCBM solid contents studied. Under these conditions, the occurrence of crystallisation coincided with the presence of nano-sized aggregates in as-spun films. At long UVO time exposure, two populations of micron-sized crystals were observed, regardless of PCBM concentration in solution: needles coexisted with smaller and more circular crystals (Figure 9), as well as nano-sized aggregates. Higher magnification imaging showed that PCBM crystals adopt a mostly regular pentagonal shape. This bimodal crystallisation has already been observed by Môn et al.[17] and the pentagonal shape of the smaller PCBM crystals have also been observed on mica substrates and associated to substrate templating.[18] Zheng *et al.* explained this 5-fold symmetry by crystal-twin formation.[18] The proportion of pentagon crystals was about 35 %. The crystal number density (Figure 8) increased with film thickness, suggesting that heterogeneous nucleation from the substrate was favoured for thicker films. The width of the crystals increased with thickness while the length of the needles decreased with thickness. This suggests that crowding prevented the crystals to grow unilaterally for thick films and thus, began to grow more isotropically. This is opposite to what we observed in the case of homogeneous nucleation, namely an increase in number crystal density for thinner films due to confinement accompanied by a decrease in crystal length but no thickening of the crystals.

Effect of light exposure on PCBM crystallization. The impact of light exposure in hindering fullerene crystallisation within a polymer matrix was previously reported and linked to a

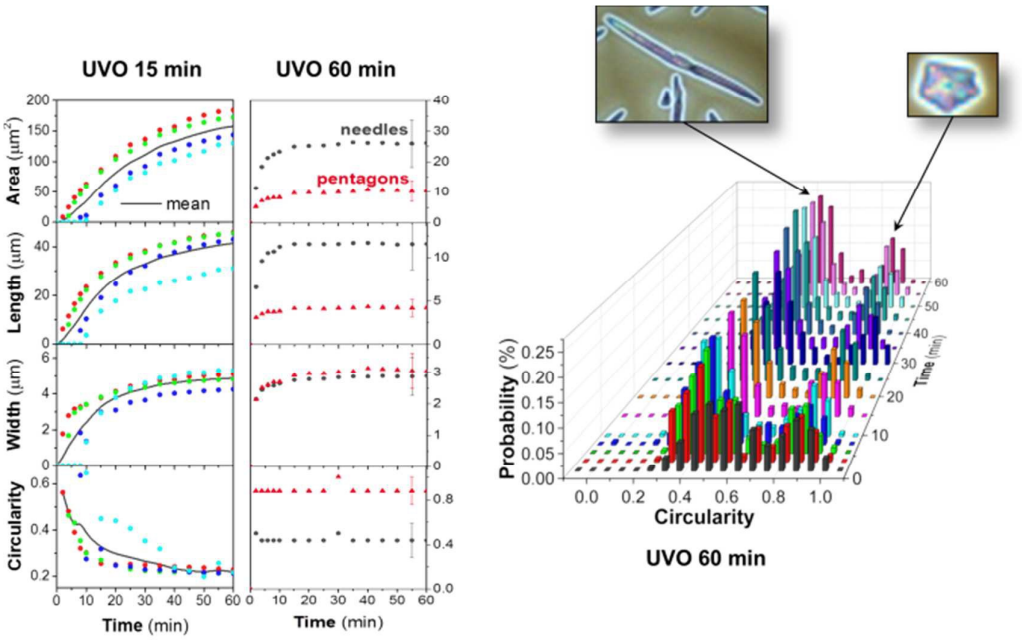

Figure 9. Area, length, width and circularity[‡] of crystals as a function of time for 3:7 RRa-P3HT:PCBM thin films cast from a 20 mg/ml PCBM in CB solution prepared at 20°C on substrates exposed to UVO for 15 and 60 min respectively. Probability distribution of the circularity for the sample cast on the substrate exposed to UVO for 60 min. The optical micrographs at different annealing times are provided in Supporting Information (Figure S8). The importance of the elapsed time before nucleation is highlighted in Supporting Information (Figure S9).

fullerene oligomerization process (in the absence of oxygen).[19] Our results corroborate these findings in the case of homogeneous nucleation, leading to a reduction in film crystallisation. However, thin films cast above the solubility limit or prepared on substrates previously exposed to UVO (60 min) provide an interesting insight into the impact on both nucleation and growth under light exposure. We considered specifically polymer:fullerene ratios for which timescales for heterogeneous and homogeneous nucleation were commensurate. Figure 10 shows optical micrographs of 3:7 RRa-P3HT:PCBM thin films cast above the solubility limit (solution of 30 mg/ml of PCBM in CB) and on a substrate exposed to UVO for 60 min. In one case, annealing was performed in the dark (under vacuum), while in the other case, annealing was performed under light exposure in a nitrogen atmosphere. For the samples prepared on substrates exposed to UVO for 15 min, the homogeneous nucleation was fully suppressed when annealing occurred under light exposure. Close inspection of these samples revealed that the heterogeneous nucleation on aggregates from solution was also affected leading to the emergence of well-defined needles that grew radially from the aggregates from solution. For the samples deposited on substrates exposed to UVO for 60 min, both homogeneous and heterogeneous nucleations were affected by exposure to light. We observed a reduction in crystals, both pentagons and needles, of about 85% (Supporting Information Figure S10). However, close inspection of these samples indicated that secondary nucleation of needles from the pentagonal crystals took place. Crystal growth seemed unaffected in the case of the samples prepared on substrates exposed to UVO for 15 min, corroborating previous measurements of growth kinetics.[14] The suppression of nucleation due to light exposure for samples treated by 60 min UVO, resulted in larger but fewer needles, by contrast with the large number (or shorter) needles observed in the dark, where the nucleation rate resulted in growth being hindered by the large number of crystals (Supporting Information Figure S11).

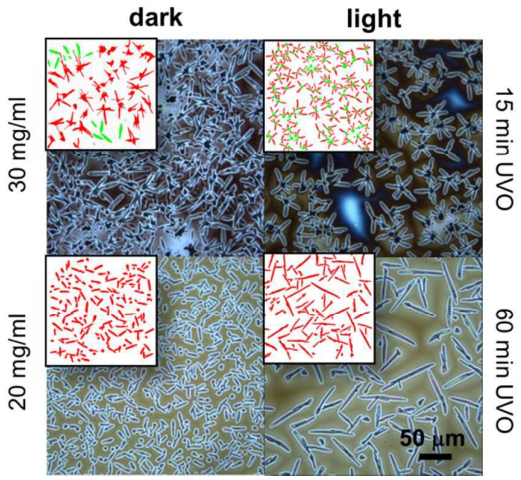

Figure 10. Optical micrographs of 3:7 RRa-P3HT:PCBM thin films cast from a 30 and 20 mg/ml PCBM in CB solution prepared at room temperature on substrates exposed to UVO for 15 and 60 min respectively. Both samples have been annealed at 160°C. Samples on the right have been exposed to light during annealing (under inert N_2 environment) while the left one has been kept in the dark (under vacuum).

3. Conclusions

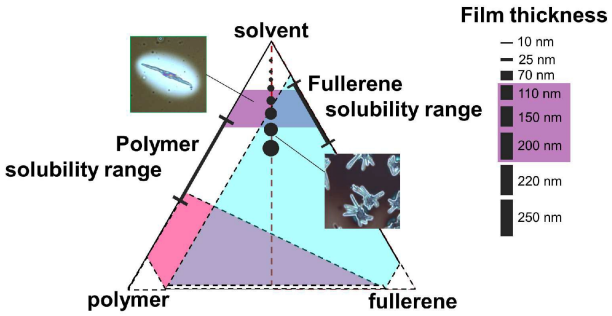

Figure 11. Scheme representing the ternary phase diagram with film thicknesses that can be achieved by spin-coating depending on the solid content in solution. The concentration range of typical OPV devices is indicated by the horizontal band (110-200 nm). Both polymer and fullerene solubility are indicated by dashed lines, with the vertical line corresponds to a drying pathway of a 1:1 polymer: fullerene mixture. The top left corner of the schematic indicates the 1-phase region, while the remaining are 2-phase regions. The scheme illustrates the control of the crystal shape that can be exerted based on the experimental results discussed.

We reported the phase diagram of RRa-P3HT/PCBM/CB focusing on conditions relevant for OPV processing. No polymer-induced fullerene aggregation was observed unlike in systems such as polystyrene mixed with C_{60} or PCBM in toluene,[10] which we rationalise in terms of interaction asymmetry. Above the solubility limit, we observed heterogeneous nucleation of PCBM in thin films, originating from PCBM aggregates in solution, by contrast with the sparse homogeneous nucleation of needles from solutions below the solubility limit. Heterogeneous nucleation and growth generally yielded needles, which grew radially from pre-formed solution aggregates. Crystal nucleation rates exhibited a sharp peak around 170°C while growth rates increased monotonically with temperature. Decreasing film thickness generally promoted homogeneous nucleation, while thicker films generally exhibited heterogeneous nucleation and greater susceptibility to surface properties. These were effectively tuned by UVO exposure and found to profoundly impact crystallisation: surface oxidation biased the nucleation process to become heterogeneous, yielding bimodal populations of needles and pentagons, whose number fraction reached 35 %. In addition, light exposure effectively suppressed the homogeneous nucleation of needles. While heterogeneous nucleation was partly inhibited, light caused secondary needles formation from pentagonal crystals, on UVO treated surfaces.

Crystal shape, density and spatial arrangement are thus strongly affected by solution behaviour, both from thermodynamics and drying pathways, and external fields. Such design opportunities are often overlooked in OPV fabrication and we thus provide a general phase diagram schematic in Figure 11, and discuss strategies for modulating PCBM crystallisation.

Device film thickness is largely controlled by the solid content in solution. Casting thin film below the solubility limit results in thicknesses up to around 150 nm, which restrict the light absorption. Previous studies[20-21] highlight the importance of PCBM crystallisation on both OPV performances and lifetime. Controlling PCBM aggregation in solution, which is both composition and time-dependent, can provide an efficient route to manipulate polymer:fullerene blend morphology without introducing foreign species that can be detrimental to electronic applications. It might also enable the decoupling of microstructure and light absorption. The non-monotonic dependence of nucleation with temperature provides a facile way of controlling crystal number density (and size), while growth increases monotonically with temperature, enabling separate control of nucleation and growth by distinct annealing stages.

Finally, even when solution engineering is not actively sought, a detailed understanding of these processes is valuable for OPV fabrication, given the plethora of film morphologies accessible for nominally "identical" systems.[25]

4. Experimental

Materials and methods. RRa-P3HT (Mw = 100 K, PDI = 3, RR = 53% and purity superior to 90%)12 and PCBM (Mw = 910.88 g/mol, purity superior to 99.5%) were purchased from Sigma Aldrich (Rieke Metals) and Solenne BV respectively and were used as purchased. All the solutions were stirred overnight except if mentioned otherwise. When the solutions were filtered, PTFE membrane filters with pore size of 0.2 μm were used. We used 〈100〉 silicon substrates (Pi-Kem Ltd) which were surface treated with a Ultraviolet UV Ozone Cleaner (Novascan) for 15 min except if mentioned otherwise. The distance between the UV lamp and the sample was kept to 2 cm for all the samples. The UV lamp spectrum as well as contact angle measurements as a function of UVO time exposure are available in the Supporting Information Figure S13 and S14. The solutions were spin-coated at 4000 rpm (acceleration 1000 rpm/s) for 2 minutes. These spin-coating parameters were chosen as lower spin speeds (<3000 rpm) yielded to variability in surface coverage and planarity and because for all the concentrations the films dried within this timescale (however, varying with film thickness and solute concentration and PCBM ratio).

Annealing protocols. The samples were either annealed at 50 mbar in a Memmert vacuum oven or in THMS 600 Linkam Thermal Cell under nitrogen. In the case of the oven, the pressure was first stabilised to 50 mbar and then 160°C was reached in 15 mins. The samples were left under vacuum until they had cooled to 25°C and then, the pressure was released. In the case of the Linkam cell, the samples underwent a temperature ramp of 150°C/min. With the exception of the temperature-dependent measurements shown in Figure 7, to ensure thermal equilibration time did not affect nucleation kinetics, the cell was sealed under nitrogen to minimise oxidation.

Light treatment. Selected samples were exposed to a 3W white light emitting diode (LED) source during thermal annealing.

Thickness measurement. We measured the thin films using a UV-visible interferometer (Filmetrics, F20-UV) calibrated with a SiO2 wafer. The n and k values to fit the measurements were taken from reference.12

UV-Vis absorption measurement. Absorption data were measured using a Perkin-Elmer Lambda 25 spectrophotometer.

Optical microscopy. Optical micrographs were acquired using an Olympus BX41M-LED reflectance mode microscope equipped with an Allied GX1050C colour camera. Time-dependent measurements were carried out using a THMS 600 Linkam Thermal Cell mounted onto the microscope stage.

Image analysis. Image analysis was carried out using ImageJ, as follows:
image contrast was first enhanced by allowing saturation of 0.4% of the pixels; colour images were then converted into 8-bit grey scale and thresholded with the modified IsoData algorithm between 0 and 135, and crystal contours were enclosed after manual inspection; built-in particle analysers were then used to extract areas, length, width and circularity of each crystal.

Acknowledgements

The authors thank Mr Prashanth Kalaiselvan for the help with the UVO time exposure measurements. A.A.Y.G thanks Dr Nikolay L. Vaklev for fruitful conversations. This work was supported by the Engineering and Physical Sciences Research Council (EPSRC) (EP/L022176/1). A.A.Y.G acknowledges EPSRC for the award of a Doctoral Prize Fellowship.

Notes and references

§ The importance of the drying pathway has been recognised by several authors and has been found to considerably impact performances.[22-24]
§§ It has to be emphasised that we use filtration to determine solubility limit therefore any aggregates smaller than 0.2 micron are considered soluble leading to an overestimation of the solubility limit. The difference in shape is likely to be due to heterogeneous nucleation from aggregates from solution smaller than 0.2 micron.
§§§. Note that we chose this time of UVO treatment since it gives us comparable results as on PEDOT:PSS which is relevant for organic electronic devices (see Figure S7 in Supporting Information).
‡ The circularity is defined as $4\pi \frac{Area}{Perimeter^2}$. Thus, the circularity ranges from 0 for infinitely elongated polygon to 1 for perfect circle.

1 A. C. Balazs, T. Emrick and T. P. Russell, *Science*, 2013, **314**, 1107-1110.
2 C. J. Brabec, M. Heeney, I. McCulloch and J. Nelson, *Chem. Soc. Rev.*, 2011, **40**, 1185-1199.
3 F. Machui, S. Abbott, D. Waller, M. Koppe and C. J. Brabec, *Macromol. Chem. Phys.*, 2011, **212**, 2159-2165.
4 F. Machui, S. Langner, X. Zhu, S. Abbott, S. and C. J. Brabec, *Sol. Energ. Mat. Sol. Cells*, 2012, **100**, 138-146.
5 L. J. Richter, D. M. DeLongchamp, F. A., Bokel, S. Engmann, K. W. Chou, A. Amassian and A. Hexemer, *Adv. Ener. Mater.*, 2015, **5**, 1400975.
6 E. Verploegen, R. Mondal, C. J. Bettinger, S. Sok, M. F. Toney, M. F. and Z. Bao, *Adv. Funct. Mater.*, 2010, **20**, 3519-3529.
7 N. D. Treat, A. Varotto, C. J. Takacs, N. Batara, M. Al-Hashimi, M. J. Heeney and M. L. Chabinyc, *J. Am. Chem. Soc.*, 2012, **134**, 15869-15679.
8 F. P. V. Koch, J. Rivnay, S. Foster, C. Müller, J. Downing, E. Buchaca-Domingo and N. Stingelin, *Prog. Polym. Sci.*, 2013, **38**, 1978-1989.
9 R. Dattani, R. Michels, A. J. Nedoma, R. Schweins, P. Westacott, K. Huber and J. T. Cabral, *Macromolecules*, 2014, **47**, 6113-6120.
10 R. Dattani and J. T. Cabral, *Soft Matter*, 2015, **11**, 3125-3131.
11 N. D. Treat and M. L. Chabinyc, *Annu. Rev. Phys. Chem.*, 2014, **65**, 59–81.
12 A. A. Y. Guilbert, M. Schmidt, A. Bruno, J. Yao, S. King, S. M. Tuladhar and J. Nelson, *Adv. Funct. Mat.*, 2014, **24**, 6972-6980.
13 E. Baka, J. E. A. Comer and K. Takács-Novák, *J. Pharm. Biomed. Anal.*, 2008, **46**, 335-341.
14 H. C. Wong, Z. Li, C. H. Tan, H. Zhong, Z. Huang, H. Bronstein, H. and J. R. Durrant, *ACS Nano*, 2014, **8**, 1297-1308.
15 Ngo, T. T., Nguyen, D. N., & Nguyen, V. T. (2012). *Adv. Nat. Sci.: Nanosci. Nanotechnol.*, 2012, **3**, 045001.
16 H. C. Wong, A. M. Higgins, A. R. Wildes, J. F. Douglas and J. T. Cabral, *Adv. Mater.,* 2013, **25**, 985-991.
17 D. Môn, A. M. Higgins, D. James, M. Hampton, J. E. Macdonald, M. B. Ward and J. Rawle, *Phys. Chem. Chem. Phys.*, 2015, **17**, 2216-2227.
18 L. Zheng, J. Liu and Y. Han, *Phys. Chem. Chem. Phys.*, 2013, **15**, 1208-1215.
19 Z. Li, H. C. Wong, Z. Huang, H. Zhong, C. Tan, W. C. Tsoi and J. T. Cabral. *Nat. Comm.*, 2013, **4**, 2227.
20 F. C. Jamieson, E. B. Domingo, T. McCarthy-Ward, M. Heeney, N. Stingelin and J. R. Durrant. *Chem. Sci.*, 2012, **3**, 485-492.
21 C. Lindqvist, J. Bergqvist, C.-C. Feng, S. Gustafsson, O. Bäcke, N. D. Treat, C. Bounioux, P. Henriksson, R. Kroon, E. Wang, Ergang, A. Sanz-Velasco, P. M. Kristiansen, N. Stingelin, E. Olsson, O. Inganäs, M. R. Andersson and C. Müller, *Adv. Ener. Mat.*, 2014, **4**, 1301437.
22 T. Wang, N. W. Scarratt, H. Yi, A. D. F. Dunbar, A. J. Pearson, D. C. Watters, T. S. Glen, A. C. Brook, J. Kingsley, A. R. Buckley, M. W. A. Skoda, A. M. Donald, R. A. L. Jones, A. Iraqi and D. G. Lidzey, *Adv. Ener. Mater.*, 2013, **3**, 505-512.
23 N. S. Güldal, T. Kassar, M. Berlinghof, T. Ameri, A. Osvet, R. Pacios, G. L. Destri, T. Unruh and C. J. Brabec, *J. Mater. Chem. C*, 2016, **4**, 2178-2186.
24 C.-H. Tan, H. C. Wong, Z. Li, D. G. Bucknall, J. R. Durrant and J. T. Cabral, *J. Mater. Chem. C*, 2015, **3**, 9551-9558.
25 M. T. Dang, L Hirsch and G Wantz, *Adv. Mat*., 2011, **23**, 3597-3602.

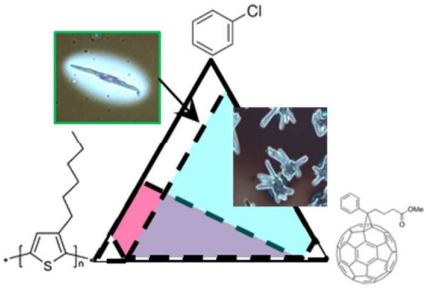

We report the impact of solution phase behaviour and external fields on PCBM crystallisation and thin film morphology.